

Designing superselectivity in linker-mediated multivalent nanoparticle adsorption

Xiuyang Xia and Ran Ni*

School of Chemistry, Chemical Engineering and Biotechnology,
Nanyang Technological University,
62 Nanyang Drive, 637459, Singapore

(Dated: October 25, 2023)

Using a statistical mechanical model and numerical simulations, we provide the design principle for the bridging energy (ξ) and linker density (ρ) dependent superselectivity in linker-mediated multivalent nanoparticle adsorption. When the bridges are insufficient, the formation of multiple bridges leads to both ξ - and ρ -dependent superselectivity. Whereas, when the bridges are excessive, the system becomes insensitive to bridging energy due to entropy-induced self-saturation and shows a superselective desorption with respect to the linker density. Counterintuitively, lower linker density or stronger bridging energy enhances the superselectivity. These findings not only help understand relevant biological processes but also open up opportunities for applications in biosensing, drug delivery, and programmable self-assembly.

Using multiple weak bindings to form effectively strong interaction, namely multivalent interactions, constitutes the cornerstone of various biological processes [1, 2]. The combinatorial entropy raised by multivalency endows the system with a superselective response to the environment [3, 4]. This plays a crucial role in determining the fate of nanomedicines in biological media: multivalent nanoparticles superselectively target cell surfaces that overexpress receptors, e.g., cancer cells or viral infections, while leaving others untouched [5, 6].

Compared to the conventional direct binding, indirect linker-mediated bridging provides new axes for regulating interactions by adjusting both the density and specificity of linkers. Here *linkers* refer to small molecules with two ends that can transiently and reversibly bind with receptors and ligands coated on hosts and guest objects forming bridges to link them. Many biological processes involve this interaction, e.g., protein degradation and transport [7], biomolecular condensates formation [8–11] and chromatin fiber reshaping [12], etc. Moreover, the linker specificity offers the *in situ* programmability that specifically “sews” a pair of building blocks by adding corresponding linkers in artificial multicomponent systems, e.g., DNA origami [13], colloidal atom-electron equivalents [14–16], artificial protein-interaction networks [17–19] and vitrimers [20, 21].

With new design elements, linker-mediated interactions also exhibit the superselectivity originating from multivalency. For example, this scheme serves as the foundation for modern sandwich immunoassays and DNA array detections [22–26]. Moreover, linker-mediated systems undergo an entropy-driven re-entrant transition with increasing linker density [15, 16]. Higher linker density promotes the bridge formation, but excessive density “over-charges” the system, preventing the formation of bridges. This process, which has recently been found to be superselective, involves the membrane repair protein annexin A5 binding to anionic lipid membranes assisted by the linker Ca^{2+} [27]. Nevertheless,

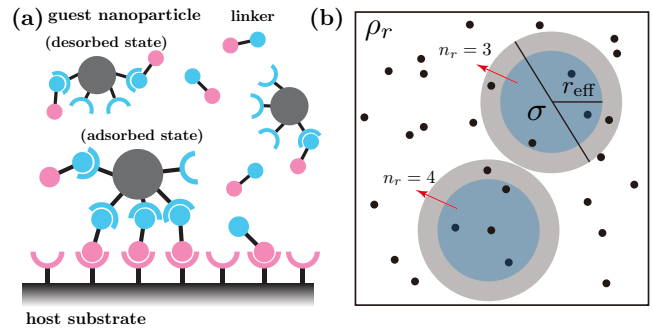


FIG. 1. **Linker-mediated adsorption of multivalent nanoparticles.** (a) Schematic representation of multivalent nanoparticles adsorption composed of a guest-linker-host sandwich. (b) Illustration of the GCMC simulation. The black dots are immobile receptors, and grey particles are adsorbed nanoparticles. Receptors within blue regions can form bridges with the ligands on nanoparticles mediated by linkers. Ligands and linkers are implicit.

due to the complex phase behavior observed in linker-mediated systems, a universal design principle for inducing superselectivity remains elusive. To this end, combining the mean-field theory of linker-mediated interactions [16] with the Langmuir-like multivalent adsorption model [4, 28], we study the bridging energy and linker density dependent superselectivity in the linker-mediated multivalent nanoparticle adsorption to offer a comprehensive guideline for designing the superselectivity in linker-mediated systems.

Model. We consider a prototypical coarse-grained model involving guest nanoparticles adsorbing on a host substrate (see Fig. 1a). Rather than the direct binding [4, 29], indirect bridgings mediated by bivalent free linkers in solution occur between the ligands on nanoparticles and the receptors on the host substrate. We define a nanoparticle *adsorbed* when it forms at least one bridge with the host substrate, and *desorbed* when no bridge is formed and it remains in the bulk solution. Each

nanoparticle is coated with n_l mobile ligands. Linkers are modeled as an ideal gas of density $\rho = e^{\beta\mu}/\Lambda^3$ with chemical potential μ , the de Broglie wavelength Λ , and $\beta = 1/k_B T$, where k_B and T are the Boltzmann constant and temperature of the system, respectively. Considering that a site on the host substrate can adsorb one guest particle at most, the probability of the nanoparticle adsorption follows the Langmuir adsorption isotherm $\theta = \langle z_g q / (1 + z_g q) \rangle_{\langle n_r \rangle}$, where z_g represents the guest nanoparticle activity in the bulk solution, which is proportional to the number density of particles and the adsorption volume [4], and $\langle \cdot \rangle_{\langle n_r \rangle}$ calculates the average over the Poisson distribution of receptors with the mathematical estimate $\langle n_r \rangle$.

Taking the desorbed state as the reference state, the adsorbed state partition function is defined as $q = e^{-\beta F_{\text{eff}}} - 1$, where the effective free energy $F_{\text{eff}} = F_{\text{ad}} - F_{\text{de}}$ originates from the formation of bridges [28]. Here, F_{ad} and F_{de} represent the free energy when a nanoparticle is adsorbed or desorbed, respectively (Fig. 1a). We assume that the two ends of linkers are specifically bound with receptors and ligands, and the partition functions $\xi_r = e^{-\beta f_r}$ and $\xi_l = e^{-\beta f_l}$ with the binding free energy f_r and f_l , respectively. The formation of a bridge causes a conformational entropy lost ΔS_{cnf} with the partition function $\xi_{\text{cnf}} = e^{k_B^{-1} \Delta S_{\text{cnf}}}$. With the saddle-point approximation, we obtain [30]

$$\beta F_{\text{eff}} = n_l \log \left(\frac{n_l - b}{n_l} \right) + n_r \log \left(\frac{n_r - b}{n_r} \right) + b, \quad (1)$$

with the equilibrium number of bridging linkers

$$b = \frac{(n_l + n_r + \Gamma^{-1}) - \sqrt{(n_l + n_r + \Gamma^{-1})^2 - 4n_l n_r}}{2}. \quad (2)$$

Here, we define the relative bridging strength

$$\Gamma = \frac{\xi_l \xi_r \xi_{\text{cnf}} \rho}{(1 + \xi_l \rho)(1 + \xi_r \rho)}, \quad (3)$$

which represents the bridging strength with respect to all unbridged states: both empty, both occupied by linkers, and only one side occupied by linkers, similar to the ligand-receptor ‘‘affinity’’ in Ref. [27].

We perform grand-canonical Monte Carlo (GCMC) simulations with implicit ligands and linkers [30–32]. As shown in Fig. 1b, we model the multivalent nanoparticles as hard disks of diameter $\sigma = 1$ and volume $s_{\text{hd}} = \pi/4$ controlled by the chemical potential μ_g . Then, we consider the explicit receptors is immobile under a Poisson distribution with number density ρ_r . A receptor can only bridge with mobile ligands on the nanoparticles within a center-to-particle-center distance r_{eff} , which quantifies the effective contact area due to curved surfaces. When the probability of the nanoparticle adsorption is small enough, we consider the total number of sites as

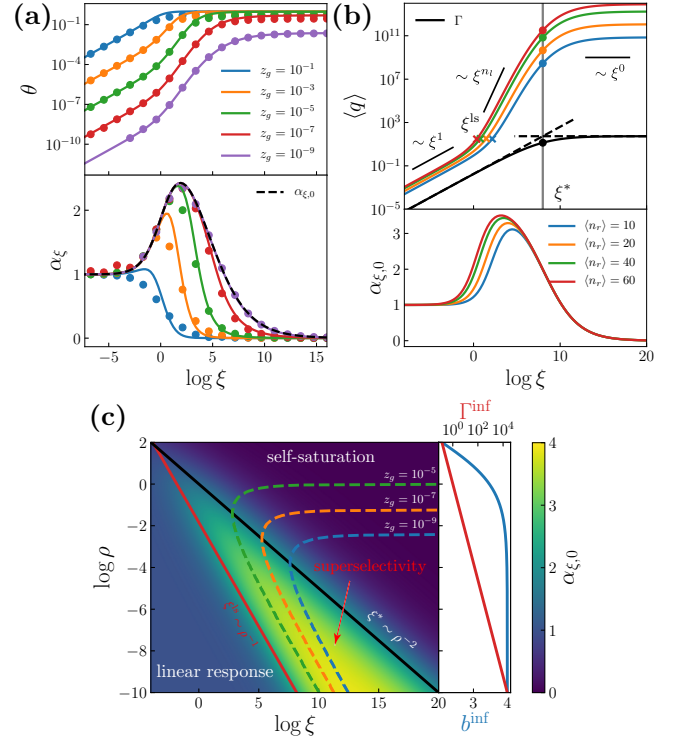


FIG. 2. ξ -dependent superselectivity. (a) θ , α_ξ and $\alpha_{\xi,0}$ as functions of $\log \xi$ at different z_g . Symbols are the simulation results, and curves are the theoretical prediction. Here $\rho = e^{-2}$, $\rho_r = 12.73$ and $r_{\text{eff}} = 0.5$. (b) Theoretical prediction of $\langle q \rangle$, Γ and $\alpha_{\xi,0}$ as a function of $\log \xi$ at $\rho = e^{-4}$ and various $\langle n_r \rangle$. Dots locate the self-saturation point ξ^* , which is the crosspoint between the dashed red lines $\Gamma = \xi \xi_{\text{cnf}} \rho$ (lower ξ) and $\Gamma = \xi_{\text{cnf}} \rho^{-1}$ (higher ξ). \times symbols indicate the transition points ξ^{ls} from linear to superlinear response. (c) Left: $\alpha_{\xi,0}$ as a function of $\log \xi$ at different $\log \rho$. Dashed curves indicate the location of minimum detectable limit $\theta = 0.1$ at different z_g . Right: at strong bridging limit, b^{inf} and Γ^{inf} as a function of $\log \rho$. In all figures, unless otherwise specified, $\langle n_r \rangle = 10$, $n_l = 4$ and $\Delta S_{\text{cnf}} = 0$.

$N_{\text{max}} = L^2/s_{\text{hd}}$ with box length L , and the average number of receptors per site $\langle n_r \rangle = \pi r_{\text{eff}}^2 \rho_r$. The guest activity is given by $z_g = e^{\beta \mu_g} s_{\text{hd}} h_0 / \Lambda^3$, with the adsorption layer thickness $h_0 = 1$.

To quantify the selectivity of nanoparticles adsorption with respect to the variation of environmental parameter χ , we generalize the definition of the multivalent selectivity in Ref. [4] as

$$\alpha_\chi = \frac{d \log \theta}{d \log \chi}. \quad (4)$$

When $\alpha_\chi > 1$, the adsorption probability increases superlinearly with the environmental parameter and $\theta \sim \chi^{\alpha_\chi}$. Similarly, a negative response $\alpha_\chi < -1$ signifies that nanoparticles desorb superlinearly.

Bridging energy dependent superselectivity. To investigate the superselective response to temperature or individual bridging energy (e.g., different base pair match-

ing [23]) of linker-mediated adsorption, we define the environmental parameter as the bridging strength of a single bridge, $\xi := \xi_l \xi_r$. We focus on the situation where the number of receptors significantly outnumbers the ligands $\langle n_r \rangle \gg n_l$. As shown in Fig. 2a, with increasing ξ , θ increases and reaches a plateau after a ξ threshold. Similar to the adsorption in direct binding, the guest nanoparticle activity z_g controls the location of the threshold [4]. When z_g is large enough, e.g., $z_g = 10^{-1}$, individual bridging saturates the host, and no ξ -dependent superselectivity exists. Decreasing z_g increases the ξ threshold and induces the formation of multiple bridges on a single nanoparticle, and the superselectivity gradually manifests, accompanied by the increased peak of α_ξ (Fig. 2a). At the zero activity limit, $\lim_{z_g \rightarrow 0} \alpha_\xi = \alpha_{\xi,0} = d \log \langle q \rangle / d \log \xi$ with $\langle q \rangle$ the adsorbed partition function under the Poisson distribution of receptors.

Intriguingly, when z_g is small, e.g., $z_g = 10^{-9}$, $\theta(\xi \rightarrow \infty)$ is significantly smaller than 1 (Fig. 2a), which is different from the direct binding of multivalent nanoparticles [4]. To understand this, we plot $\langle q \rangle$ and $\alpha_{\xi,0}$ as functions of ξ in Fig. 2b. We find that the ξ -response can be divided into three parts. At the weak bridging limit, i.e., $\xi < \xi^{\text{ls}}$, the bridging strength is too weak to induce cooperative effects, and the linear response $\alpha_{\xi,0} \approx 1$ appears. When $\xi > \xi^{\text{ls}}$, stronger bridging strength triggers the formation of multiple bridges, a power-law response $\alpha_{\xi,0} \approx n_l$ appears, indicating the ξ -dependent superselectivity. Here, larger multivalency naturally promotes the number of bridges and enhances selectivity. The bridging strength $\xi^{\text{ls}} = n_l^{1/(n_l-1)} / (\langle n_r \rangle \xi_{\text{cnf}} \rho)$ indicates the transition from linear to superlinear response [30]. Moreover, when ξ further increases, $\langle q \rangle$ saturates with no selectivity $\alpha_{\xi,0} \approx 0$. At the large ξ limit, the relative bridging strength $\Gamma^{\text{inf}} \approx \xi_{\text{cnf}} \rho^{-1} \sim \xi^0$ dictated solely by entropy. The entropy induced *self-saturation* effect makes $\langle \theta \rangle$ unable to reach 1 at the low temperature limit with small z_g . As shown in Fig. 2b, the superlinear ξ -response terminates at $\xi^* \sim \rho^{-2}$.

Next, we investigate the ξ -dependent superselectivity at different ρ . The contourplot of $\alpha_{\xi,0}$ in $\log \xi - \log \rho$ plane is shown in Fig. 2c, where superselectivity ($\alpha_{\xi,0} > 1$) appears between $\xi^{\text{ls}} \sim \rho^{-1}$ and $\xi^* \sim \rho^{-2}$. Interestingly, with decreasing ρ , both of the range width and value of $\alpha_{\xi,0}$ increases. At a given ρ , $\Gamma^{\text{inf}} \sim \rho^{-1}$, hence, the maximum bridge number b^{inf} is ρ -dependent, instead of n_l in direct binding [4]. Smaller ρ brings stronger Γ^{inf} to form more bridges. The bridge number, which can be seen as the effective valence, determines the cooperativity triggering the superselectivity. Meanwhile, lower ρ also needs stronger ξ to reach the regime of self-saturation, which broadens the superselective range.

Experimentally, the detectable range of θ is limited by measurement techniques or environmental noise. For example, in scanometric DNA array detections, parti-

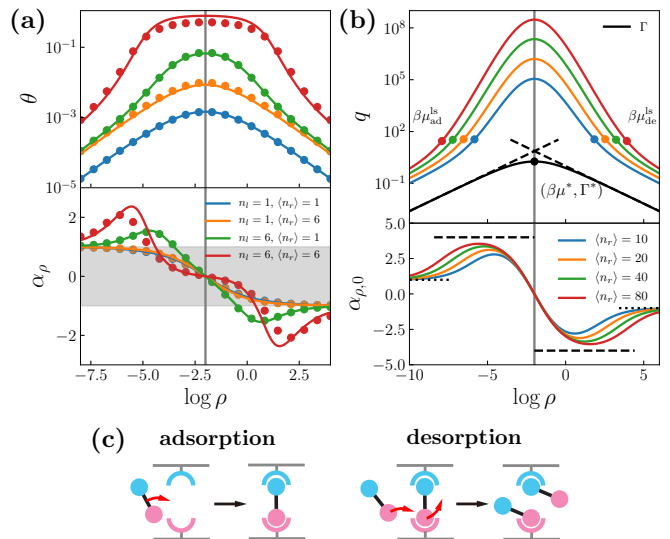


FIG. 3. ρ -dependent superselectivity. (a) θ , α_ρ and $\alpha_{\rho,0}$ as functions of $\log \rho$ for mono- and multivalent ligands for $\langle n_r \rangle = 1$ and 6. Grey area indicates no superselectivity. Here $\xi_l = \xi_r = e^2$ and $r_{\text{eff}} = 0.5$. (b) Theoretical prediction of $\langle q \rangle$, Γ and $\alpha_{\rho,0}$ as functions of $\log \rho$ at $\xi_l = \xi_r = e^{-2}$ with different $\langle n_r \rangle$. Black dots locate the transition point ρ^* , which are the crosspoints between the dashed red lines $\Gamma = \xi_l r \rho$ (adsorption regime) and $\Gamma = \xi_{\text{cnf}} \rho^{-1}$ (desorption regime). Other colored symbols indicates the transition points $\rho_{\text{ad}}^{\text{ls}}$ and $\rho_{\text{de}}^{\text{ls}}$ from linear to superlinear response in adsorption and desorption regimes, respectively. (c) Illustration of adsorption and desorption process with increasing linker density where bridges are insufficient (left) and excessive (right).

cle probes must polymerize to form network structures, causing a noticeable color shift [23]. As shown in Fig. 2c, assuming a minimum detectable limit $\theta = 0.1$ and at a given ρ , lower z_g makes the system unable to reach the detectable limit due to the self-saturation effect, eliminating the detectable superselectivity. Superselectivity can be only observed at certain range of z_g , different from the direct binding where low z_g typically enhance the superselectivity [33, 34].

Linker density dependent superselectivity. As shown in Fig. 3a, with increasing linker density ρ , θ initially increases and then decreases in all cases. The peak location of θ corresponding to the targeted linker density is $\rho^* = \xi^{-1/2}$ [30], and below and above this peak are defined as the adsorption and desorption regimes, respectively. As shown in Fig. 3b and c, we find that the adsorption-desorption transition originates from the non-monotonic dependence of Γ on ρ . When $\rho < \rho^*$, we have $\Gamma \approx \xi \xi_{\text{cnf}} \rho$, where the bridges are insufficient, and the adsorption process involves sequential insertions of linkers and formation of bridges. Conversely, in the desorption regime, we have $\Gamma \approx \xi_{\text{cnf}} \rho^{-1}$, where the bridges is excessive, and the desorption process involves free linkers attacking bridges and forming dangling bonds.

We consider the linker density ρ as the environmental

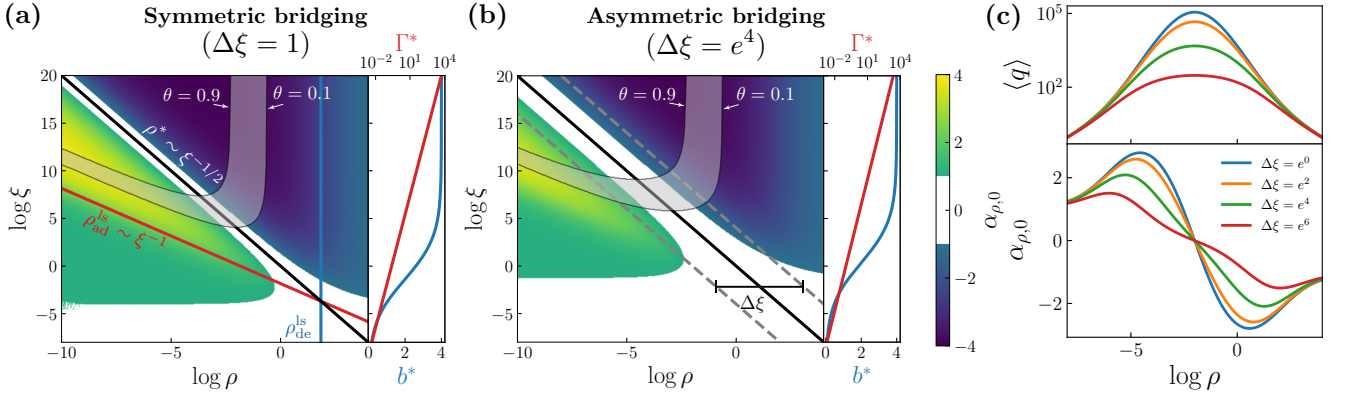


FIG. 4. ρ -dependent superselectivity with symmetric and asymmetric bridgings. (a,b) Left: $\alpha_{\rho,0}$ as a function of $\log \rho$ at different $\log \xi$, right: b^* and Γ^* as functions of $\log \xi$. The bridging is (a) symmetric $\Delta\xi = 1$ and (b) asymmetric $\Delta\xi = e^4$ with $\Delta\xi = \xi_l/\xi_r$, respectively. Black lines locate ρ^* , red and blue solid lines locate ρ_{ad}^{ls} and ρ_{de}^{ls} , respectively. Grey solid lines indicates the location $\theta = 0.1$ and 0.9 at $z_g = 10^{-6}$, and grey dashed lines indicate the boundary of the plateau induced by asymmetric bridging. (c) $\langle q \rangle$ and $\alpha_{\rho,0}$ as functions of $\log \rho$ at $\xi = e^4$ with various $\Delta\xi$.

parameter with the corresponding selectivity parameter α_{ρ} . As shown in Fig. 3a, the superselective adsorption and desorption $|\alpha_{\rho}| > 1$ occurs when the guest nanoparticles are multivalent, e.g., $n_l = 6$, where multiple bridges can form. Moreover, the superselectivity also occurs at $\langle n_r \rangle = 1$, which implies that the spatial fluctuation of receptors promotes ρ -dependent sensitivity, since it involves larger n_r and q . We use zero-activity selectivity $\alpha_{\rho,0}$ to analyse the origin of ρ -dependent superselectivity. As shown in Fig. 3b, we obtain four modes of $\langle q \rangle$ dependence. At the limit of both low and high linker densities, weak bridging $\Gamma \rightarrow 0$ can not trigger cooperativity, and $|\alpha_{\rho,0}| \approx 0$. The strongest relative bridging strength occurs at ρ^* and $\Gamma^* = \Gamma(\rho^*) = \xi_{cnf}/(\xi_l^{-1/2} + \xi_r^{-1/2})^2$, which increases with $\xi_{l/r}$. The adsorption process involving the formation of multiple bridges triggers the cooperativity characterized by a power-law dependence with $|\alpha_{\mu,0}|^{\max} = n_l$. Moreover, $|\alpha_{\mu,0}|^{\max}$ also increases with increasing the receptor concentration on substrate $\langle n_r \rangle$ (Fig. 3b). Hence, the linker-mediated multivalent adsorption provides a clean and shutterlike “off-on-off” response targeting a specific linker density or density window.

When the bridging energy is symmetric, i.e., $\Delta\xi = \xi_l/\xi_r = 1$, as shown in Fig. 4a, the targeted linker density $\rho^* \sim \xi^{-1/2}$ decreases with increasing the bridging strength ξ , and the stronger bridging broadens the density range of superselectivity with the lower and upper bounds $\rho_{ad}^{ls} \sim \xi^{-1}$ and $\rho_{de}^{ls} \sim \xi^0$, respectively. Moreover, stronger bridging leads to higher relative bridging strength with more bridges formed and higher selectivity. Similar to the ξ -dependent superselectivity, with a minimum detectability limit, the ρ -dependent superselectivity cannot be observed at very low guest activity z_g or weak ξ .

Combining both ξ - and ρ -dependent superselectivity,

we propose a general design rule for the superselective adsorption of linker-mediated multivalent nanoparticles. When bridging is insufficient, i.e., $\xi\rho^2 < 1$, both ξ - and ρ -superselectivity appears at $\xi\rho > n_l^{1/(n_l-1)}/(\langle n_r \rangle \xi_{cnf})$. In the excess bridging region, i.e., $\xi\rho^2 > 1$, entropy dictates the adsorption and the corresponding superselectivity. The entropy induced self-saturation effect eliminates the ξ dependence, and the superselective desorption appears with increasing ρ when $\rho < (\langle n_r \rangle \xi_{cnf})/n_l^{1/(n_l-1)}$. We note that the guest nanoparticle activity z_g can linearly shift the adsorption point and determine the saturation point, which can be experimentally controlled by adjusting the nanoparticle density and/or introducing extra repulsion or attraction between nanoparticles and the substrate [34].

Asymmetric bridging scheme. Lastly, we investigate the effect of asymmetric bridging on the superselectivity by mismatching the binding energy of two different linker ends, i.e., $\Delta\xi = \xi_l/\xi_r \neq 1$. In Fig. 4b, we plot the ρ -dependent superselectivity of an asymmetric bridging scheme with the asymmetry degree $\Delta\xi = \xi_l/\xi_r = e^4$. Compared to the symmetric bridging, i.e., $\Delta\xi = 1$ in Fig. 4a, $|\alpha_{\rho,0}|^{\max}$ decreases significantly when the bridging energy is not strong. In Fig. 4c, one can see that increasing $\Delta\xi$ decreases the peaks of $\langle q \rangle$, while $\langle q \rangle$ in the linear response regime remains unaffected at both low and high linker density limits. The decreased $\langle q \rangle$ indicates less number of bridges formed, which leads to a decrease in $|\alpha_{\rho,0}|^{\max}$ at fixed ξ (Fig. 4b and S1). Moreover, as shown in Fig. 4b, the asymmetric bridging introduces a plateau with indiscriminate adsorption of ρ , of which the width is $\Delta\xi$. This explains that the melting temperature of crystals consisting of asymmetric linker-mediated DNA coated colloids remains constant in certain range of linker density [35]. The asymmetric bridging also decreases the $\alpha_{\xi,0}^{\max}$ because of the emergence of a new scaling region

with $\alpha_{\xi,0} \approx n_l/2$ (Fig. S2).

Discussion. The interplay between energy and entropy in linker-mediated interactions results in rich phase behaviour, making the superselectivity arising from multivalency intricate and distinct from the direct binding. Here, we have investigated both the bridging energy and linker density dependent superselectivity in linker-mediated multivalent nanoparticle binding. We theoretically estimate the bridge number and adsorption probability and elucidate the origins of superselectivity in various scenarios. The intrinsic feature of linker-mediated interaction is captured by a key parameter, the relative bridging strength, Γ . Larger Γ and multivalency lead to multiple bridges formed between host and guest nanoparticles, yielding a cooperative multivalent effect and superselectivity accordingly. We estimate the parameter bounds as guiding principles for designing the linker-mediated superselectivity. Our theory suggests that for any experimental parameter χ , if $\Gamma \sim \chi$, then $\alpha_{\chi}^{\max} > 1$. Moreover, our finding may also shed lights on the understanding of fundamental physics in biological systems, such as client recruitment in biomolecular condensates [36–38].

This work is supported by the Academic Research Fund from the Singapore Ministry of Education Tier 1 Gant (RG59/21).

* r.ni@ntu.edu.sg

- [1] M. Mammen, S.-K. Choi, and G. M. Whitesides, *Angew. Chem. Int. Ed.* **37**, 2754 (1998).
- [2] J. Huskens, *Curr. Opin. Chem. Biol.* **10**, 537 (2006).
- [3] P. I. Kitov and D. R. Bundle, *J. Am. Chem. Soc.* **125**, 16271 (2003).
- [4] F. J. Martinez-Veracoechea and D. Frenkel, *Proc. Natl. Acad. Sci. U.S.A.* **108**, 10963 (2011).
- [5] M. E. Davis, J. E. Zuckerman, C. H. J. Choi, D. Seligson, A. Tolcher, C. A. Alabi, Y. Yen, J. D. Heidel, and A. Ribas, *Nature* **464**, 1067 (2010).
- [6] P.-A. Koenig, H. Das, H. Liu, B. M. Kümmerer, F. N. Gohr, L.-M. Jenster, L. D. Schiffelers, Y. M. Tesfamariam, M. Uchima, J. D. Wuerth, *et al.*, *Science* **371**, eabe6230 (2021).
- [7] M. Schapira, M. F. Calabrese, A. N. Bullock, and C. M. Crews, *Nat. Rev. Drug Discovery* **18**, 949 (2019).
- [8] E. S. F. Rosenzweig, B. Xu, L. K. Cuellar, A. Martinez-Sanchez, M. Schaffer, M. Strauss, H. N. Cartwright, P. Ronceray, J. M. Plitzko, F. Förster, *et al.*, *Cell* **171**, 148 (2017).
- [9] J. B. Rayman, K. A. Karl, and E. R. Kandel, *Cell reports* **22**, 59 (2018).
- [10] J. J. Bouchard, J. H. Otero, D. C. Scott, E. Szulc, E. W. Martin, N. Sabri, D. Granata, M. R. Marzahn, K. Lindorff-Larsen, X. Salvatella, *et al.*, *Mol. Cell* **72**, 19 (2018).
- [11] J.-K. Ryu, C. Bouchoux, H. W. Liu, E. Kim, M. Minamino, R. de Groot, A. J. Katan, A. Bonato, D. Maren-duzzo, D. Michieletto, *et al.*, *Sci. Adv.* **7**, eabe5905 (2021).
- [12] I. Malhotra, B. Oyarzún, and B. M. Mognetti, *Biophys. J.* **120**, 1247 (2021).
- [13] P. W. Rothmund, *Nature* **440**, 297 (2006).
- [14] M. Girard, S. Wang, J. S. Du, A. Das, Z. Huang, V. P. Dravid, B. Lee, C. A. Mirkin, and M. Olvera de la Cruz, *Science* **364**, 1174 (2019).
- [15] J. Lowensohn, B. Oyarzún, G. N. Paliza, B. M. Mognetti, and W. B. Rogers, *Phys. Rev. X* **9**, 041054 (2019).
- [16] X. Xia, H. Hu, M. P. Ciamarra, and R. Ni, *Sci. Adv.* **6**, eaaz6921 (2020).
- [17] D. W. Sanders, N. Kedersha, D. S. Lee, A. R. Strom, V. Drake, J. A. Riback, D. Bracha, J. M. Eeftens, A. Iwanicki, A. Wang, *et al.*, *Cell* **181**, 306 (2020).
- [18] M. Heidenreich, J. M. Georgeson, E. Locatelli, L. Rovigatti, S. K. Nandi, A. Steinberg, Y. Nadav, E. Shimoni, S. A. Safran, J. P. Doye, *et al.*, *Nat. Chem. Biol.* **16**, 939 (2020).
- [19] S. K. Nandi, D. Österle, M. Heidenreich, E. D. Levy, and S. A. Safran, *Phys. Rev. Lett.* **129**, 128102 (2022).
- [20] Q.-L. Lei, X. Xia, J. Yang, M. Pica Ciamarra, and R. Ni, *Proc. Natl. Acad. Sci. U.S.A.* **117**, 27111 (2020).
- [21] X. Xia, P. Rao, J. Yang, M. P. Ciamarra, and R. Ni, *JACS Au* **2**, 2359 (2022).
- [22] A. Voller, D. Bidwell, and A. Bartlett, *Bull. World Health Organ.* **53**, 55 (1976).
- [23] T. A. Taton, C. A. Mirkin, and R. L. Letsinger, *Science* **289**, 1757 (2000).
- [24] Y. C. Cao, R. Jin, and C. A. Mirkin, *Science* **297**, 1536 (2002).
- [25] R. Jin, G. Wu, Z. Li, C. A. Mirkin, and G. C. Schatz, *J. Am. Chem. Soc.* **125**, 1643 (2003).
- [26] D. Lukatsky and D. Frenkel, *The J. Chem. Phys.* **122** (2005).
- [27] T. Curk, G. V. Dubacheva, A. R. Brisson, and R. P. Richter, *J. Am. Chem. Soc.* **144**, 17346 (2022).
- [28] S. Angioletti-Uberti, *Phys. Rev. Lett.* **118**, 068001 (2017).
- [29] C. Linne, D. Visco, S. Angioletti-Uberti, L. Laan, and D. J. Kraft, *Proc. Natl. Acad. Sci. U.S.A.* **118**, e2106036118 (2021).
- [30] Supplementary Materials.
- [31] G. V. Dubacheva, T. Curk, R. Auzély-Velty, D. Frenkel, and R. P. Richter, *Proc. Natl. Acad. Sci. U.S.A.* **112**, 5579 (2015).
- [32] X. Xia, G. Zhang, M. Pica Ciamarra, Y. Jiao, and R. Ni, *JACS Au* **3**, 1385 (2023).
- [33] S. Wang and E. E. Dormidontova, *Phys. Rev. Lett.* **109**, 238102 (2012).
- [34] H. T. Phan, D. Lauzon, A. Vallée-Bélisle, S. Angioletti-Uberti, J. Leblond Chain, and S. Giasson, *Proc. Natl. Acad. Sci. U.S.A.* **120**, e2208377120 (2023).
- [35] J. Lowensohn, A. Hensley, M. Perlow-Zelman, and W. B. Rogers, *Langmuir* **36**, 7100 (2020).
- [36] S. F. Banani, A. M. Rice, W. B. Peeples, Y. Lin, S. Jain, R. Parker, and M. K. Rosen, *Cell* **166**, 651 (2016).
- [37] A. T. Christy, H. Kusumaatmaja, and M. A. Miller, *Phys. Rev. Lett.* **126**, 028002 (2021).
- [38] P. Yang, C. Mathieu, R.-M. Kolaitis, P. Zhang, J. Messing, U. Yurtsever, Z. Yang, J. Wu, Y. Li, Q. Pan, *et al.*, *Cell* **181**, 325 (2020).